Materials Transactions, Vol. 61, No. 3 (2020) pp. 449 to 454

Deposition-Temperature Dependence of Vortex Pinning Property in $YBa_2Cu_3O_7$+ $BaHfO_3$ Films*[1]

Tomoya Horide[1], Kenta Torigoe[1,*2], Ryusuke Kita[2], Ryota Nakamura[1,*2], Manabu Ishimaru[1], Satoshi Awaji[3] and Kaname Matsumoto[1]

[1]*Department of Materials Science and Engineering, Kyushu Institute of Technology, Kitakyushu 804-8550, Japan*
[2]*Graduate School of Integrated Science and Technology, Shizuoka University, Hamamatsu 432-8561, Japan*
[3]*Institute for Materials Research, Tohoku University, Sendai 980-8577, Japan*

Improvement of critical current density (J_c) in magnetic fields is required in $YBa_2Cu_3O_7$ films, and process parameters should be optimized for controlling pinning centers. In the present study, a deposition temperature was varied in pulsed laser deposition of $YBa_2Cu_3O_7$+$BaHfO_3$ films to control the nanorod structure, and its influence on J_c was analyzed. The $YBa_2Cu_3O_7$+$BaHfO_3$ film deposited at 850°C exhibited pinning force maximum ($F_{p,max}$) as high as 413 GN/m^3 at 40 K, while the $F_{p,max}$ for the deposition temperature of 850°C at 77 K was smaller than that in the $YBa_2Cu_3O_7$+$BaHfO_3$ film deposited at 900°C. A critical temperature decreased and matching field increased with decreasing the deposition temperature. Increase in deposition temperature is effective in improving the $F_{p,max}$ in high temperatures, since the critical temperature and matching field dependences of J_c value dominate the $F_{p,max}$. On the other hand, low deposition temperature improves the $F_{p,max}$ in low temperatures since the F_p shift in accordance with matching field is dominant to the $F_{p,max}$. Thus, the deposition temperature should be set in pulsed laser deposition of $YBa_2Cu_3O_7$ films containing nanorods considering the J_c variation with critical temperature and matching field.
[doi:10.2320/matertrans.MT-M2019303]

(Received October 17, 2019; Accepted December 16, 2019; Published February 25, 2020)

Keywords: *$YBa_2Cu_3O_7$, vortex pinning, critical current density, nanorod, thin film*

1. Introduction

For development of high-performance $REBa_2Cu_3O_7$ (REBCO; RE = Y, Nd, Sm, Gd etc.) superconducting tapes, improvement of critical current density (J_c) is required.[1)] Introduction of pinning centers can improve J_c, and nanocomposite structures containing nanorods or nanoparticles are effective in improving vortex pinning in REBCO superconducting tapes. Pulsed laser deposition (PLD)[2)] and metal organic chemical vapor deposition (MOCVD)[3)] are the most used method for fabricating REBCO tapes, and $BaMO_3$ (BMO; M = Zr, Sn, Hf etc.) nanorods,[4–7)] which work as strong pinning centers, can be introduced into the REBCO tapes and films using these methods. The vortex pinning properties of nanorods are determined by several structural parameters such as nanorod density, length, interface structure, and strain etc. The nanorod density significantly affects the pinning properties in magnetic field, since the vortex density increases with increasing magnetic field.[8)] The length and tilt of nanorods determine the vortex volume which is accommodated by a nanorod, namely the pin potential. Furthermore, the interface structure affects an elementary pinning force.[9)] It has also been reported that the strain of matrix affects the critical temperature (T_c) by varying the oxygen vacancy formation energy.[10)] To achieve high J_c in the REBCO tapes and films containing nanorods, the process parameters should be optimized to control these factors.

Supply of atoms from the plume, surface diffusion, nucleation and growth occur under non-equilibrium conditions in the case of PLD. Deposition temperature, laser condition, target composition etc. should be optimized to control these phenomena, when high quality single phase films are fabricated using PLD.[11–13)] The growth of nanocomposite film is more complicated, because the nanocomposite structure is formed with complex process comprising diffusion of atoms, nucleation and growth of matrix and second phase, and coalescence of the islands. The nanorod structure is significantly changed by the PLD conditions such as the deposition temperature and the deposition rate as well as the selection of matrix and nanorod material. In order to control the nanorod structure in REBCO, RE = Y, Nd, Sm, Eu, Gd, etc. for matrix, and M = Zr, Hf, Sn etc. for nanorod have been investigated. Furthermore, it has been reported that the nanorod structure and the J_c characteristics are controlled by changing the PLD conditions. Among them, the deposition temperature is one of the most important parameters. It has been reported that the size, density, and length of nanorods strongly depend on the deposition temperature: The nanorods are cut and tilted[14,15)] and the density of the nanorods is increased[16)] with lowering the deposition temperature. These indicate that the deposition temperature should be optimized to control the nanorod structure and to achieve high J_c.

In this study, we focus on the deposition temperature in fabricating $YBa_2Cu_3O_7$+$BaHfO_3$ (YBCO+BHO) films using PLD. A magnetic field dependence of J_c significantly varied with the deposition temperature, and high J_c values were obtained at 40 K in the film prepared at moderately low temperature. We analyze the J_c values based on T_c and matching field, and the deposition-temperature dependence of vortex pinning is discussed in the YBCO+BHO films. Based on the results, structure and process designs on nanorod are discussed to achieve high J_c in YBCO+BMO films.

*1This Paper was Originally Published in Japanese in J. Japan Inst. Met. Mater. **83** (2019) 320–326.
*2Graduate Student, Kyushu Institute of Technology

Table 1 Parameters of the YBCO+BHO films prepared in the present study.

	Thickness /nm	$T_{c,0}$ /K	J_c (77 K,0T) /MA/cm^2	J_c (77K, 5T) /MA/cm^2	n value at 77 K, 2 T	J_c (20K, 9T) /MA/cm^2
YBCO+BHO(900)	150	87.9	2.3	0.34	13.2	3.3
YBCO+BHO(890)	120	88.0	2.1	0.28	10.8	4.2
YBCO+BHO(850)	140	86.1	2.6	0.28	9.9	6.8
YBCO+BHO(830)	200	83.5	0.26	0.012	4.0	2.3

2. Experimental

Sample preparation was performed using PLD. The target was a YBCO+BHO mixed target, whose BHO content was fixed at 4.7 vol%. The oxygen partial pressure was 26 Pa, and the film thickness is shown in Table 1. The deposition temperature was varied between 830°C and 900°C. After the deposition, the films were cooled to 200°C in an oxygen atmosphere of 55000 Pa in 1 hour, and the films were removed from the chamber at 100°C or below. Here, YBCO+BHO(X) means a YBCO+BHO film prepared at X°C. Transmission electron microscopy (TEM) observation was performed to clarify the nanorod structure. A bridge having a width of 90 µm and a length of 1 mm was formed on the films by photolithography and H_3PO_4 wet etching, and superconducting properties were evaluated using Physical Property Measurement System. T_c and irreversible temperature (T_{irr}) were evaluated by measuring a temperature dependence of electrical resistance. A current density-electric field (J-E) curve was measured to evaluate J_c. Furthermore, the J_c in the YBCO+BHO(850) was measured in temperatures of 65 K and 40 K and magnetic fields up to 16 T using the 20 T superconducting magnet in Institute of Materials Research, Tohoku University. The magnetic field angles for the magnetic fields parallel to the *ab* plane and the *c*-axis are defined as −90° and 0°, respectively. 1 µV/cm was used as a criterion to determine the J_c and T_{irr}. Furthermore, the n value was obtained in the range of 10–100 µV/cm assuming the relationship of $E \sim J^n$.

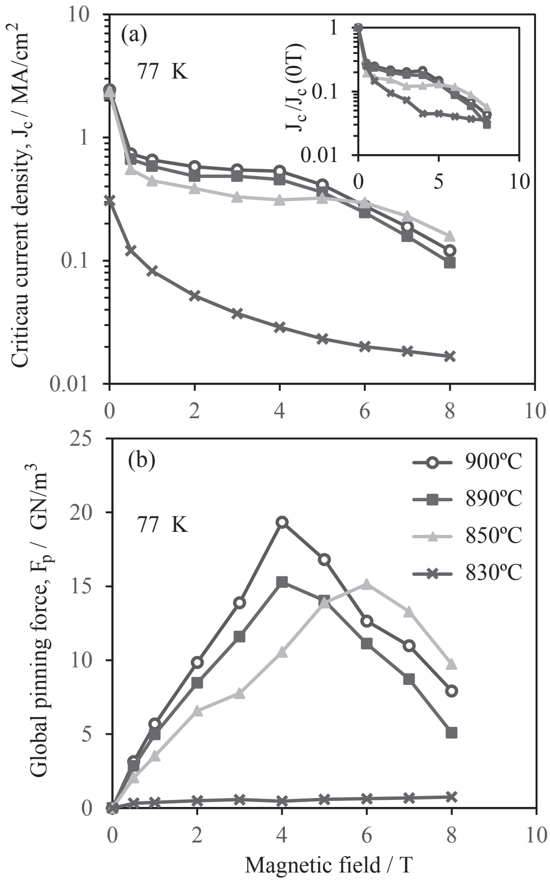

Fig. 2 Magnetic field dependences of (a) J_c and (b) F_p at 77 K for the YBCO+BHO films.

3. Results

The cross-sectional TEM image of the YBCO+BHO(850) is shown in Fig. 1. The nanorods with a spacing of 15–20 nm and a diameter of ~6 nm are elongated through the film thickness. The matching field (B_Φ) is roughly estimated to be ~6.8 T from the spacing of the nanorods. From a report on deposition-temperature dependence of the nanorod structure,[15] it is considered that the nanorods are elongated through the thickness at the deposition temperatures higher than 850°C.

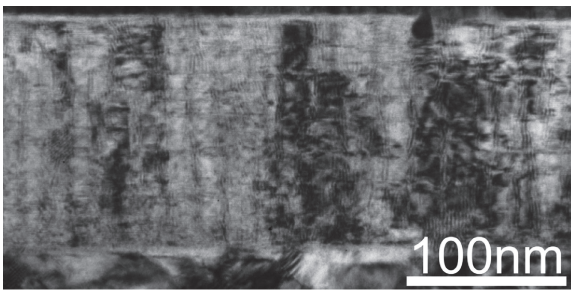

Fig. 1 TEM image of the YBCO+BHO(850) film.

Figure 2 shows a magnetic field dependence of J_c at 77 K in the films. When the deposition temperature was 850–900°C, the J_c at 0 T was about 2 MA/cm^2. On the other hand, the J_c for YBCO+BHO(830) was 0.3 MA/cm^2 at 0 T. The YBCO+BHO(890) and YBCO+BHO(900) films exhibit almost the same J_c-B curves, and the J_c decreases above 4 T. In the YBCO+BHO(850), the magnetic field dependence of J_c is different from those in the YBCO+BHO(890) and

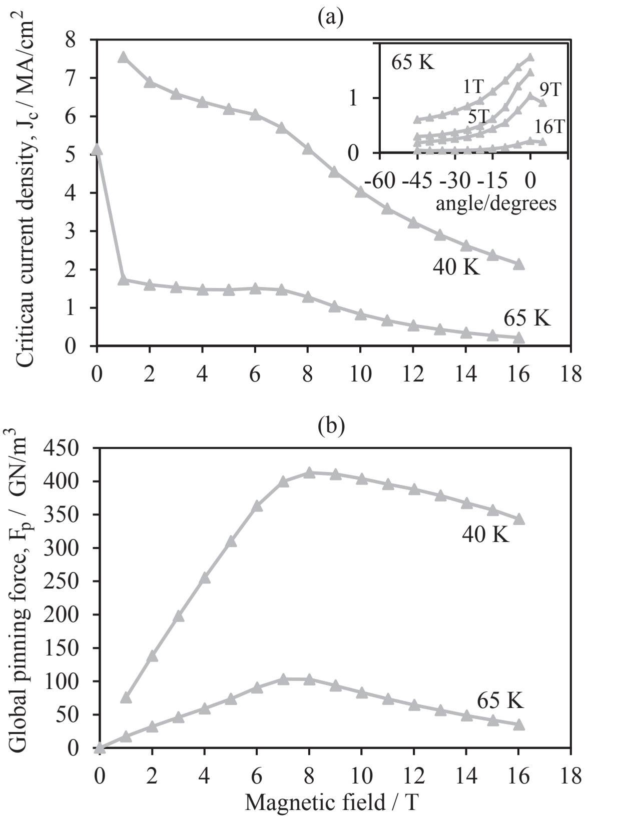

Fig. 3 Magnetic field dependences of (a) J_c and (b) F_p in temperatures of 40 K and 65 K for the YBCO+BHO(850) film.

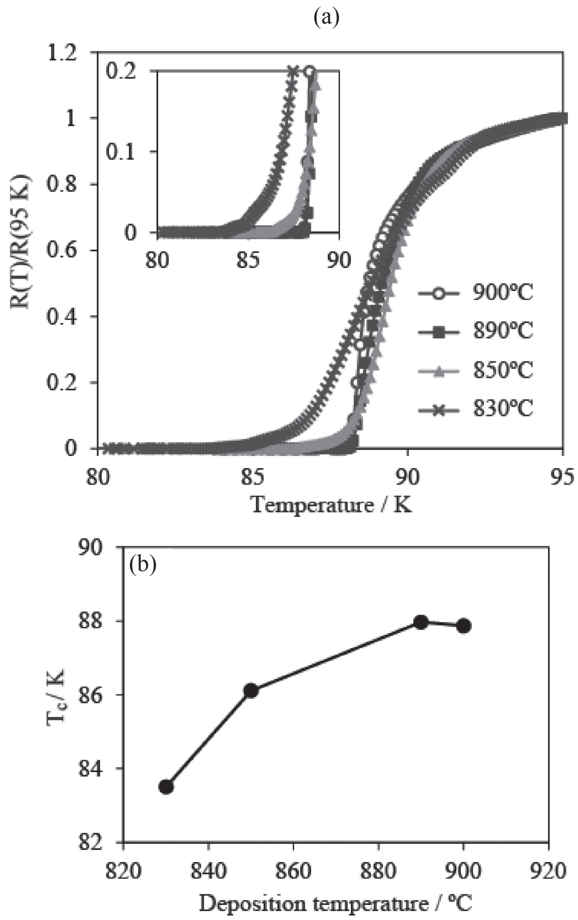

Fig. 4 (a) $R(T)/R(95\,K)$-T curves in the YBCO+BHO films. Inset shows the enlarged view. (b) Deposition-temperature dependence of T_{c0}.

YBCO+BHO(900), and J_c starts to decrease at 6 T. Furthermore, the magnetic field dependence of the global pinning force ($F_p = J_c \times B$) is shown in Fig. 2(b). The F_p for deposition temperatures of 890°C and 900°C exhibits the maximum value at 4 T, and the largest value at 77 K in this study is 19.3 GN/m^3 in the YBCO+BHO(900). The YBCO+BHO(850) exhibits a $F_{p,max}$ (maximum value of F_p) of 15.1 GN/m^3 at 6 T. On the other hand, in the YBCO+BHO(830), the J_c and F_p at 77 K are one or more orders smaller than those in the other films. Thus, it was found that the J_c at 77 K strongly depends on the deposition temperature, and the $F_{p,max}$ at 77 K decreases with lowering the deposition temperature. Table 1 also shows the J_c of 20 K and 9 T. At high temperature (77 K) and low magnetic field, the YBCO+BHO(900) exhibits a high J_c, but J_c becomes higher in the YBCO+BHO(850) with decreasing temperature and with increasing magnetic field. In the YBCO+BHO(830), the J_c at 77 K is extremely small, but the J_c at 20 K and 9 T is comparable to that in the other films.

From the results in Fig. 2, high J_c is expected at low temperature and high magnetic field in the YBCO+BHO(850). The J_c characteristics of YBCO+BHO(850) at 65 K and 40 K are shown in Fig. 3. The F_p of YBCO+BHO(850) exhibits the maximum at 7–8 T in temperatures of 65 K and 40 K. These are almost the same as the magnetic field at which $F_{p,max}$ was observed at 77 K, showing that the matching field determines the $F_{p,max}$ and the peak field. The value of $F_{p,max}$ is 103 GN/m^3 at 65 K and 413 GN/m^3 at 40 K. Figure 3 also shows an angular dependence of the J_c at 65 K in the YBCO+BHO(850). A large c-axis peak in the YBCO+BHO(850) shows that the nanorod worked as a strong c-axis correlated pinning centers.

The matching field (B_Φ) and T_c are important parameters for J_c characteristics. Figure 4 shows a resistance-temperature (R-T) curve of the films. The resistance started to decrease near 90 K, and became zero at 88–83 K. Sharp superconducting transition was observed around 88 K for the YBCO+BHO(900) and the YBCO+BHO(890). However, the YBCO+BHO(850) and YBCO+BHO(830) films exhibited a two-step superconducting transition, and this tendency was remarkable in the YBCO+BHO(830). It is considered that the two-step transition is caused by a compositional deviation due to the deposition at the low temperature. The deposition-temperature dependence of T_{c0} is shown in Fig. 4(b). As is observed in the R-T curves, T_{c0} decreases with decreasing the deposition temperature, and the significant decrease in T_{c0} is caused by the two-step superconducting transition.

T_{irr}-B and $(1 - T_{irr}/T_c)$-B curves are shown in Fig. 5(a) and (b). T_{irr} decreases with increasing magnetic field, but its tendency varies after exhibiting a shoulder at ~3.5–7 T. The T_{irr}-B behavior for the high magnetic field side and for the low magnetic field side does not depend on the deposition temperature, but the magnetic field at which the shoulder is observed strongly depends on the deposition temperature. It is known that the shoulder is observed at B_Φ in T_{irr}-B curve.[8)]

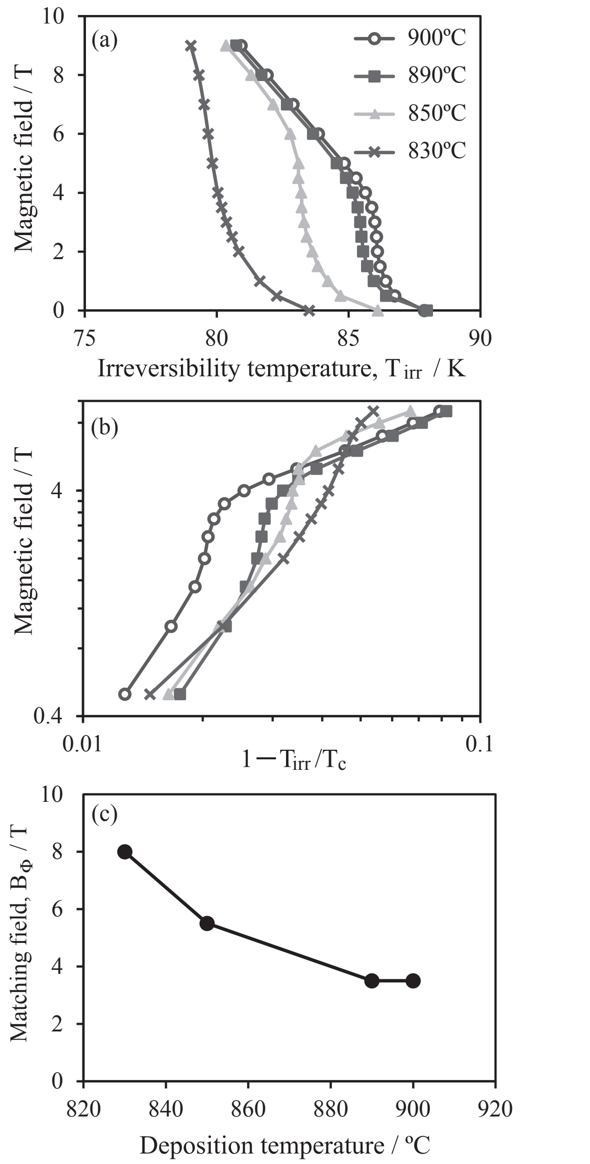

Fig. 5 (a) T_{irr}-B curves and (b) $(1 - T_{irr}/T_c)$-B curves for the YBCO+BHO films. (c) Deposition-temperature dependence of B_Φ in the YBCO+BHO films.

A dependence of B_Φ on the deposition temperature is shown in Fig. 5(c), demonstrating that the nanorod spacing decreases as the diffusion length decreases with lowering the deposition temperature. The difference between the B_Φ values determined from the TEM and the T_{irr} shoulder may be due to the accuracy for measuring the nanorod spacing in the cross-sectional observation. Furthermore, the F_p peak in low temperature may possibly be affected by contribution of the random pinning. Also in the previous report, the T_c has decreased and the B_Φ has increased with decreasing the deposition temperature in YBCO+BHO.[17] The difference between the present and previous results are due to slight difference in controlling the substrate temperature and the growth rate, but it seems that the present tendency of T_c and B_Φ to the deposition temperature is similar to that in the previous report.

4. Discussion

Table 2 compares the present results with the high J_c values reported in literatures.[18–20] The $F_{p,max}$ value of 15 GN/m^3 at 77 K is not so large compared with the results in the previous reports. On the other hand, the $F_{p,max}$ values of 400–407 GN/m^3 have been observed in SmBCO+BHO at 40 K,[18,19] and the present $F_{p,max}$ value of 413 GN/m^3 at 40 K is one of the highest values. Thus, the high $F_{p,max}$ was successfully obtained especially at 40 K in the present YBCO+BHO(850). The reason for the high $F_{p,max}$ value is discussed based on T_c and B_Φ.

4.1 Magnetic field dependence of J_c

At 77 K, the $F_{p,max}$ for the YBCO+BHO(900) and YBCO+BHO(890) was larger than that for the YBCO+BHO(850). The size of nanorod decreases with decreasing the deposition temperature, and the diameter of nanorod was about 6 nm in the YBCO+BHO(850). When the nanorod size is smaller than the vortex size, the vortex volume which is accommodated by a nanorod may determine the pin potential. However, the J_c(0 T) obtained from the pin potential is much larger than the experimental value, suggesting that not only the depinning from the nanorod but also vortex excitation such as half loop or double kink determine the J_c.[21] Actually, the J_c(0 T) at 77 K is comparable in the YBCO+BHO(900), YBCO+BHO(890), and YBCO+BHO(850), and the difference in nanorod size does not affect the J_c(0 T). The previous study also showed that the effect of nanorod size decreases with decreasing temperature, and the effect of nanorod size disappears below 77 K.[22] The result in this study is consistent with this previous conclusion. Thus, the influence

Table 2 High J_c and F_p values in the present study and literatures.[18–21] A peak field denotes the magnetic field where $F_{p,max}$ is observed. *The F_p was obtained from the reported J_c-B curves.

Sample	T_c / K	B_Φ / T	$F_{p,max}$ (77 K) / GN/m^3	Peak field (77 K) / T	$F_{p,max}$ (40 K) / GN/m^3	Peak field (40 K) / T
YBCO +BHO(850)	86.1	6.8	15.1	6	413	8
SmBCO +BHO [18]	91.1	5.8	32.5	5	400	5
SmBCO +BHO [19]	91	9.9	14.2	6	407	10
GdBCO +BHO [20]	89.1	4.1	22.5	5.5	285	7
(Gd,Y)BCO +20%Zr [3]	90		22*	3-5*	365*	5-9*

of nanorod size is not dominant to the difference of J_c in this study.

The B_Φ dependence of $J_c(B)/J_c(0\,T)$ is discussed. In Fig. 2, $J_c(B < B_\Phi)/J_c(0\,T)$ is large in the YBCO+BHO(900) whose B_Φ is small. It has been reported that $J_c(B < B_\Phi)/J_c(0\,T)$ decreases with increasing B_Φ in YBCO+BMO.[8] When the vortices move between the nanorods by the double kink or half loop excitation, the vortex excitation becomes more significant with increasing B_Φ, that is, with decreasing the nanorod spacing. The vortex motion has been discussed based on the n value[23] and creep analysis.[14] The n values at 77 K and 2 T are shown in Table 1, indicating that the n value is small for low deposition temperature. The result on n value also supports the conclusion that the vortex excitation becomes significant in the case of narrow nanorod-spacing, namely the case of low deposition temperature.

On the other hand, when B_Φ increases, it becomes possible to pin high-density vortices, so high J_c can be maintained even in high magnetic fields. J_c is almost constant at 1–7 T in the YBCO+BHO(850) because there are sufficient pinning sites. When the magnetic field increases and all the pinning centers are occupied by vortices, the vortices are pinned by elastic interaction between vortices, and J_c decreases rapidly. Since the region of single vortex pinning by the nanorods was extended to high magnetic field, $F_{p,max}$ shifted to the high magnetic field, and as a result, the $F_{p,max}$ at low temperature became large in the YBCO+BHO(850).

4.2 Influence of T_c on nanorod pinning

It is expected that T_c also significantly affects J_c. Figure 6(a) shows a T_c dependence of $J_c(77\,K,\ 0\,T)$ in the YBCO+BMO films. In addition to the results of this study, the results of the literature which is shown in Table 2[18–20] are also shown. The results for the films with different B_Φ are compared in Fig. 6(a), since the $J_c(0\,T)$ is not affected by the matching field. In order to take account of the two-step transition, T_c^{str} was obtained by extrapolating the sharp decrease in R-T curve at $T < T_c^{onset}$ to $R = 0$. T_{c0} is determined by the weakest point along the superconducting path. On the other hand, T_c^{str} represents the superconducting transition with excluding anomaly of the inhomogeneously weakened point. J_c is given by the voltage generation when current flows in the entire superconducting region, suggesting that T_c^{str}, not T_{c0} is suitable parameter for discussing J_c. Actually, it has already been discussed that the J_c values can be explained by T_c^{str} rather than T_{c0}.[17] Although some results deviated from the tendency, the $J_c(77\,K,\ 0\,T)$ tends to increase with increasing T_c regardless of the sample. The reason for the deviation in some samples is reduction in effective current flowing path, or the change in nanorod shape (e.g. the inclined growth of nanorod at low deposition temperature). Furthermore, Fig. 6(b) shows the $J_c(40\,K,\ 3\,T)$-T_c (T_c^{str}) for the samples in the present study, the samples reported in the previous studies,[17] and the samples of Table 2. Because the in-field J_c is strongly affected by matching field, Fig. 6(b) shows the results for $B_\Phi = 4$–$7\,T$. Here, the result in Ref. 19 is excluded from Fig. 6(b) because its B_Φ of $\sim$10 T is slightly larger than the B_Φ in Fig. 6(b). Similarly to the $J_c(77\,K,\ 0\,T)$, the $J_c(40\,K,\ 3\,T)$ decreases with decreasing T_c (T_c^{str}).

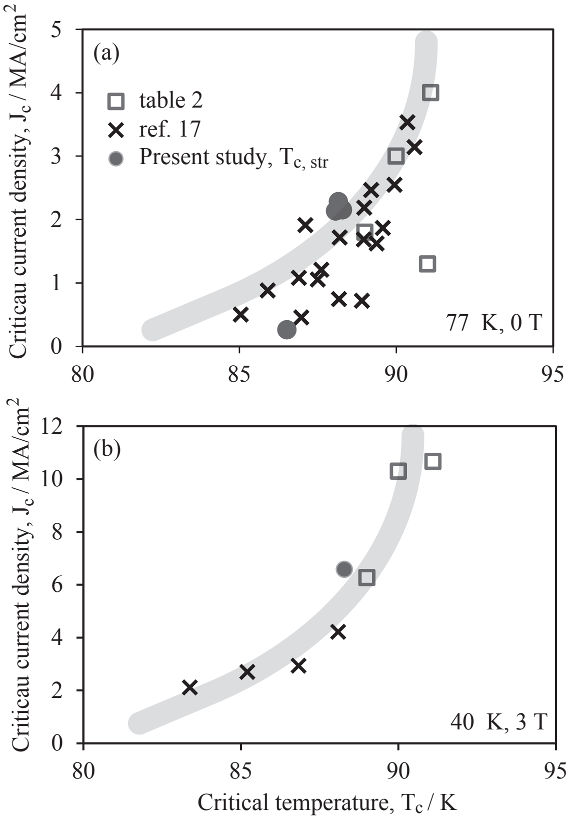

Fig. 6 (a) T_c (T_c^{str}) dependence of $J_c(77\,K,\ 0\,T)$ in the present YBCO+BHO films, our previous report, and the samples in Table 2. (b) T_c (T_c^{str}) dependence of $J_c(40\,K,\ 3\,T)$ for the samples with matching field of 4–7 T.

4.3 Nanorod structure design for improving $F_{p,max}$

These analyses show that the $F_{p,max}$ is determined by the B_Φ dependence of $J_c(B < B_\Phi)/J_c(0\,T)$, the peak shift of $F_{p,max}$, and the T_c effect. The $F_{p,max}$ at 77 K in the present study was smaller than those in the literature which is discussed in Table 2. Both the T_c dependence of J_c value and B_Φ dependence of $J_c(B < B_\Phi)/J_c(0\,T)$ significantly affect the $F_{p,max}$ in high temperatures near 77 K. The $F_{p,max}$ shifts to high magnetic field due to large B_Φ in the YBCO+BHO(850), but this cannot compensate the effect of T_c and $J_c(B < B_\Phi)/J_c(0\,T)$. Therefore, in order to obtain high $F_{p,max}$ in high temperatures, moderate (or low) matching field and high T_c are required, and this situation can be achieved by increasing the deposition temperature.

On the other hand, the high $F_{p,max}$ at 40 K was obtained for the deposition temperature of 850°C in spite of low T_c (T_c^{str}). In this study, the $F_{p,max}$ was observed in slightly higher magnetic field in the YBCO+BHO(850) than in the previous reports.[3,18,20] The high $F_{p,max}$ was obtained in the YBCO+BHO(850) because the peak shift in F_p dominantly increased $F_{p,max}$. This indicates that the $F_{p,max}$ in low temperatures can be enhanced by increasing B_Φ even if T_c is slightly lowered. This is achieved by moderately low deposition-temperature.

Thus, this study demonstrates that the J_c characteristics can be controlled by changing B_Φ and T_c, and that optimization of B_Φ and T_c is needed depending on temperature and magnetic field for J_c measurement. Furthermore, structure control such as the hybrid pinning[21,24] and the control of interface and strain at the atomic scale is promising for further improvement of J_c.

5. Summary

The YBCO+BHO films were prepared using PLD, where the deposition temperature was changed between 830 and 900°C to control the nanorod structure. The highest $F_{p,max}$ at 77 K (= 19.3 GN/m^3) was obtained for the deposition temperature of 900°C, but the high $F_{p,max}$ at 40 K was 413 GN/m^3 in the film deposited at 850°C. As the deposition temperature decreased, T_c decreased and B_Φ increased. The films with high T_c and low B_Φ can achieve high $F_{p,max}$ in high temperatures such as 77 K, while the film with high B_Φ exhibits high $F_{p,max}$ at low temperatures such as 40 K even if the T_c is slightly low. While the former situation of high T_c and low B_Φ is achieved in high deposition temperature, the latter situation of slightly low T_c and high B_Φ is achieved in moderately low deposition temperature. Depending on temperature and magnetic field for measurement and application, the deposition temperature should be varied based on T_c and B_Φ to enhance the J_c.

Acknowledgements

This work was partially supported by Grant-in-Aid for Scientific Research (B) (18H01478). The measurement was partially performed at High Field Laboratory for Superconducting Materials Institute for Materials Research, Tohoku University (17H0047).

REFERENCES

1) X. Obradors and T. Puig: Supercond. Sci. Technol. **27** (2014) 044003.
2) V. Chepikov, N. Mineev, P. Degtyarenko, S. Lee, V. Petrykin, A. Ovcharov, A. Vasiliev, A. Kaul, V. Amelichev and A. Kamenev: Supercond. Sci. Technol. **30** (2017) 124001.
3) V. Selvamanickam, M.H. Gharacheshmeh, A. Xu, Y. Zhang and E. Galstyan: Supercond. Sci. Technol. **28** (2015) 072002.
4) J.L. MacManus-Driscoll, S.R. Foltyn, Q.X. Jia, H. Wang, A. Serquis, L. Civale, B. Maiorov, M.E. Hawley, M.P. Maley and D.E. Peterson: Nat. Mater. **3** (2004) 439–443.
5) A. Goyal, S. Kang, K.J. Leonard, P.M. Martin, A.A. Gapud, M. Varela, M. Paranthaman, A.O. Ijaduola, E.D. Specht, J.R. Thompson, D.K. Christen, S.J. Pennycook and F.A. List: Supercond. Sci. Technol. **18** (2005) 1533–1538.
6) P. Mele, K. Matsumoto, T. Horide, A. Ichinose, M. Mukaida, Y. Yoshida, S. Horii and R. Kita: Supercond. Sci. Technol. **21** (2008) 032002.
7) H. Tobita, K. Notoh, K. Higashikawa, M. Inoue, T. Kato, M. Yoshizumi, T. Izumi and Y. Shiohara: Supercond. Sci. Technol. **25** (2012) 062002.
8) T. Horide, K. Taguchi, K. Matsumoto, N. Matsukida, M. Ishimaru and R. Kita: Appl. Phys. Lett. **108** (2016) 082601.
9) C. Cantoni, Y. Gao, S.H. Wee, E.D. Specht, J. Gazquez, J. Meng, S.J. Pennycook and A. Goyal: ACS Nano **5** (2011) 4783–4789.
10) T. Horide, F. Kametani, S. Yoshioka, T. Kitamura and K. Matsumoto: ACS Nano **11** (2017) 1780–1788.
11) T.J. Jackson and S.B. Palmer: J. Phys. D **27** (1994) 1581–1594.
12) S. Proyer, E. Stangl, M. Borz, B. Hellebrand and D. Bauerle: Phys. C **257** (1996) 1–15.
13) B. Dam, J.H. Rectoer, J.M. Huijbregtse and R. Griessen: Phys. C **305** (1998) 1–10.
14) B. Maiorov, S.A. Baily, H. Zhou, O. Ugurlu, J.A. Kennison, P.C. Dowden, T.G. Holesinger, S.R. Foltyn and L. Civale: Nat. Mater. **8** (2009) 398–404.
15) S. Horii, H. Kai, M. Mukaida, K. Yamada, R. Teranishi, A. Ichinose, K. Matsumoto, Y. Yoshida, R. Kita, J. Shimoyama and K. Kishio: Appl. Phys. Lett. **93** (2008) 152506.
16) T. Ozaki, Y. Yoshida, Y. Ichino, Y. Takai, A. Ichinose, K. Matsumoto, S. Horii, M. Mukaida and Y. Takano: J. Appl. Phys. **108** (2010) 093905.
17) T. Horide, S. Nagao, R. Izutsu, M. Ishimaru, R. Kita and K. Matsumoto: Supercond. Sci. Technol. **31** (2018) 065012.
18) S. Miura, Y. Yoshida, Y. Tsuchiya, Y. Ichino, S. Awaji, A. Ichinose, K. Matsumoto, A. Ibi, T. Izumi and M. Iwakuma: Appl. Phys. Express **10** (2017) 103101.
19) S. Miura, Y. Yoshida, Y. Ichino, A. Tsuruta, K. Matsumoto, A. Ichinose and S. Awaji: Supercond. Sci. Technol. **28** (2015) 114006.
20) S. Awaji, Y. Yoshida, T. Suzuki, K. Watanabe, K. Hikawa, Y. Ichino and T. Izumi: Appl. Phys. Express **8** (2015) 023101.
21) T. Horide, T. Kawamura, K. Matsumoto, A. Ichinose, M. Yoshizumi and Y. Shiohara: Supercond. Sci. Technol. **26** (2013) 075019.
22) T. Horide, N. Matsukida, M. Ishimaru, R. Kita, S. Awaji and K. Matsumoto: Appl. Phys. Lett. **110** (2017) 052601.
23) H. Yamasaki and K. Endo: IEEE Trans. Appl. Supercond. **25** (2015) 7500504.
24) G. Ercolano, M. Bianchetti, S.C. Wimbush, S.A. Harrington, H. Wang, J.H. Lee and J.L. MacManus-Driscoll: Supercond. Sci. Technol. **24** (2011) 095012.